Experimental airfoil characterization under tailored turbulent conditions

Hendrik Heißelmann, Joachim Peinke and Michael Hölling
ForWind – Institute of Physics, University of Oldenburg, 26111 Oldenburg, GER
E-mail: hendrik.heisselmann@uni-oldenburg.de

Abstract. Studies of the impact of turbulent inflow conditions on the airfoil characteristics were performed within the EU FP7 project AVATAR. The aim of this study is to provide data for the validation of simulations and the improvement of engineering tools.
Chord-wise pressure distributions and highly-resolved force data of the wind turbine dedicated DU 00-W-212 profile were measured in the wind tunnel in two tailored turbulent inflow conditions generated with an active grid. A sinusoidal and an intermittent pattern with customized inflow angle fluctuations were generated providing two significantly different distributions of reduced frequencies. The obtained pressure distributions and polars from the unsteady patterns are compared to the laminar baseline case.

1. Introduction

Historically airfoil characterizations in aerospace engineering are performed in specially designed wind tunnels with highly laminar flow conditions. The negligence of unsteady effects on the airfoil performance in these conditions, triggered many investigations of airfoils in unsteady flows. These were mainly motivated by helicopter applications, where the angular velocity of the rotor is significantly larger than the mean wind flow and the small scale turbulence in particular. The flow around the blades is therefore dominated by the rotation and yields distinct reduced frequencies, which characterize the degree of unsteadiness [1]. To tackle the mechanisms of dynamic stall, experiments in unsteady conditions are often based on the generation of periodic angle of attack (AoA) variations either by periodically pitched airfoils or by periodically modified inflows [2, 3]. However, wind turbines usually operate in highly turbulent conditions due to the nature of the atmospheric boundary layer [4] and the state of turbine operation (e.g. half wakes, yaw misalignment). Since the rotational velocities of the rotor are significantly lower, atmospheric turbulence has an increased impact and adds to the unsteadiness of the flow from rotational effects, e.g. due to tower shadowing. The rotor blades consequently face a variety of different flow situations, which may be associated with different scales. Rather than one characteristic reduced frequency, these conditions result in a wider range of reduced frequencies characterizing the problem [5]. Attempts to include turbulence in the experimental airfoil characterization have been undertaken in some studies using various classical grids to create homogeneous isotropic turbulence [6, 7] and fractal grids to include features of atmospheric turbulence [8, 9]. These setups were used to modify the velocity variations by means of the turbulence intensity, but were not designed to generate defined AoA variations at the airfoil position. To overcome this limitation, a wind tunnel setup was developed at the University of Oldenburg, which allows for

the generation of specifically tailored turbulence patterns by means of an active grid [10, 11] in order to measure the airfoil characteristics in turbulent inflow. Customized velocity variations or inflow angle variations can be produced and even scaled time series from other measurements can be synthesized to a certain extent.
In a first campaign within the EU FP7 project AVATAR, measurements on a DU 00-W-212 airfoil were performed in laminar and different turbulent inflows at Re$\approx 500,000$. A follow-up campaign was carried out for the same inflow patterns at $Re \approx 1,000,000$. The results presented in the following are entirely based on the lower Re number data. Although it is beyond the scope of this paper, the preliminary analysis of the laminar airfoil polars indicate good agreement for both Reynolds numbers.

2. Experimental Setup

Experimental airfoil characterizations were performed on a DU00-W-212 model in the return-type acoustic wind tunnel at the University of Oldenburg. The investigated airfoil model with a chord of 300 mm is vertically mounted inside the closed test section with cross-section of 1.0 m $\times$ 0.805 m (w $\times$ h) and 2.6 m length, which is sketched in Figure 1. The airfoil has an aspect ratio of 2.68 and is fixed to two rotating plates at its ends, which are fitted flush with the test section floor and ceiling. Two axes support the model at quarter chord and each axis is connected to a three-component load cell. The top axis is also equipped with a torque sensor and a stepper motor to control the geometric angle of attack α, which is monitored by an angle encoder at the bottom mount.
The reference wind speed is measured with a Setra C239 pressure gauge connected to Pitot-static tubes in the wind tunnel contraction. A combined sensor for the meteorological data (ambient pressure p, temperature T, rel. humidity rH) is situated downstream the airfoil at the end of the closed test section (Fig. 1).

Chord-wise pressure distributions were measured via 48 pressure taps distributed in a staggered alignment along the model surface as depicted in Figure 2 to avoid wake interference. One tap is located at the leading edge, 25 taps along the upper surface, 21 taps along the lower surface and one tap is located at the trailing edge. The pressure taps with 0.3 mm diameter are connected to a system of three synchronized multi-channel scanners, which record the pressure at 100 Hz sampling frequency. The data acquisition with all sensors (pressure scanners, load cells, torque sensor, met sensors) are synchronized by means of a LabVIEW software and measurements are started upon a common trigger.

The presented experiments were performed in laminar inflow conditions as well as in customized turbulent flow. Classical airfoil polars were obtained as a baseline case by mounting the closed test section of the wind tunnel directly to the outlet nozzle. An active grid was inserted between nozzle and test section in order to generate the reproducible, customized inflow patterns for the turbulent measurements [11, 4]. The grid features 16 individually movable shafts with attached flaps [10], of which only the 9 vertical shafts were moved during the airfoil experiment. All horizontal shafts remained in open position (least blockage) to render a quasi two-dimensional turbulence pattern with customized inflow angle variations.
A velocity-specific transfer function was used to relate grid movement and resulting flow angle in order to implement two different motion patterns of the shafts – so-called grid protocols – for the generation of sinusoidal and intermittent inflow angle fluctuations in the flow. While the sinusoidal protocol is meant to generate a flow with fixed amplitude at one single dominant frequency, the intermittent protocol covers a broader range of frequencies with varying amplitudes. Amplitudes and frequencies can be tuned in both cases by adapting the grid protocol, i.e. choice of flap angles and rotational velocities.

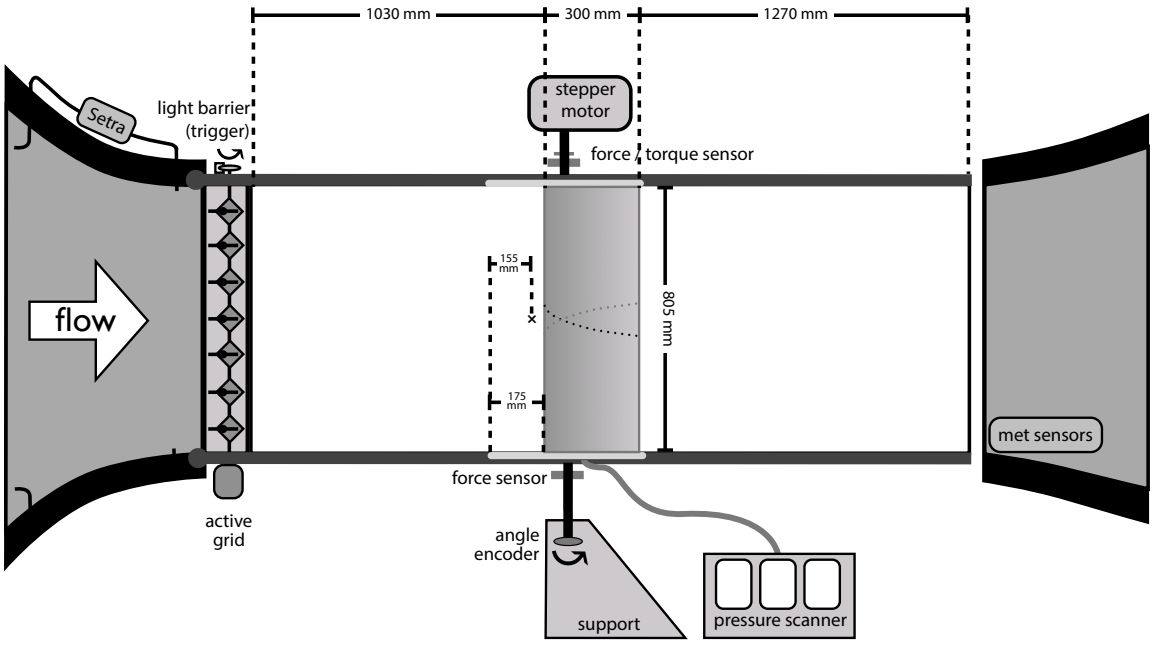

Figure 1. Sketch of the closed test section setup for the airfoil characterization (side view). The airfoil model is mounted vertically on two axes with attached force sensors. A torque sensor is mounted on the top axes. The reference wind speed is measured upstream the active grid with a Setra pressure gauge and ambient conditions are obtained from a combined (p, T, rH)-sensor downstream.

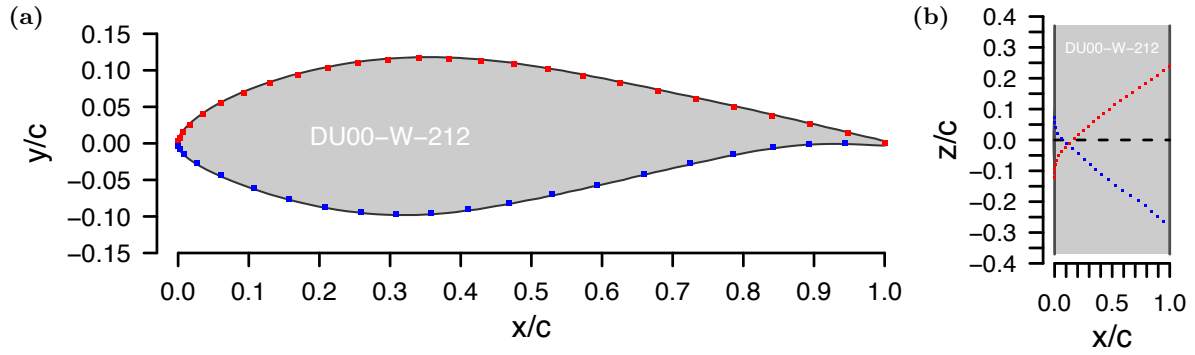

Figure 2. Position of the pressure taps on the upper side (red; incl. LE & TE) and lower side (blue) of the airfoil model. (a) Profile view of the DU00-W-212, (b) excerpt of the span around its center line (dashed).

3. Inflow Characteristics

The flow field of the wind tunnel has been characterized in the empty test section for all inflow cases at the airfoil position using hot-wire anemometry. In laminar operation without installed active grid the background turbulence level $I_u = \sigma_u/\bar{u}$ has been found to be lower than 0.3% within the wind speed range of 10 m/s to 50 m/s. A mean velocity $u \approx 26$ m/s was used for the experiments presented here, which corresponds to a Reynolds numbers $Re_c = \frac{\bar{u}\ c}{\nu}$ of about 500,000 based on the airfoil chord c.

Two different turbulent inflow conditions have been generated with the active grid using a

sinusoidal grid protocol, as well as an intermittent protocol. They have been assessed by means of a x-wire probe on the centerline located 20 mm upstream the position of the airfoil's leading edge ($\times$ mark in Fig. 1). The mean flow quantities, i.e. velocity $\bar{u}$, standard deviation σ_u and turbulence intensity I_u, of all considered inflow types are listed in Table 1 along with Reynolds number Re_c and reduced frequency [1]

$$\kappa = \frac{2\pi \cdot f \cdot c/2}{\bar{u}}, \tag{1}$$

where applicable. The resulting turbulence intensities of 3.8% and 5% for intermittent and sinusoidal inflow, respectively, are comparable to values found in measurements at the blade during a field experiment ($I_u \approx 2.1\%$) in a low turbulence site and can be considered reasonable for higher turbulence sites or wake situations.

Table 1. Characteristic quantities of the three different inflows from hot-wire measurements on the center line.

inflow	Re_c	$\bar{u}$ [m/s]	σ_u [m/s]	I_u [%]	κ
laminar	538,000	26.9	0.06	0.2	–
sinusoidal	518,000	25.9	1.3	5.0	0.18
intermittent	540,000	27.0	1.0	3.7	≤ 0.5

The sinusoidal protocol yields inflow angle fluctuations $\Delta\varphi = \pm\, 6^\circ$ with a distinct frequency f =5 Hz at the airfoil position (Fig. 3 (a)), which corresponds to a reduced frequency of $\kappa \approx 0.18$. The intermittent inflow pattern lacks such a pronounced periodicity and thus exhibits no single reduced frequency κ. Instead, structures corresponding to a wider range of reduced frequencies are apparent in the turbulent inflow (Fig. 3 (b)). A detailed distribution of the occurring reduced frequencies in the inflow can be gained from the reduced frequency power spectra in Figure 4 in order to grasp the level of unsteadiness. As expected due to the occurrence of a single excitation frequency, the sinusoidal inflow features a relatively sharp peak at $\kappa = 0.18$, while the intermittent inflow is characterized by a power distribution over a range of reduced frequencies extending up to $\kappa = 0.5$. It is therefore closer to what is expected in natural flows associated with wind energy applications [5].

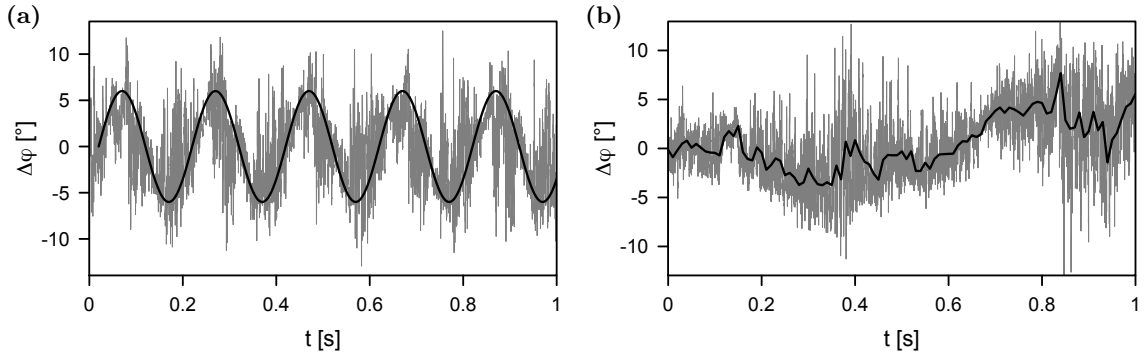

Figure 3. One second excerpts of inflow angles with sinusoidal protocol (a) and intermittent protocol (b). The time series (gray) of the sinusoidal protocol is fitted with a sinus function with 5 Hz frequency and 6° amplitude (black), while the averaged time series over 0.01 s is plotted for the intermittent protocol (black).

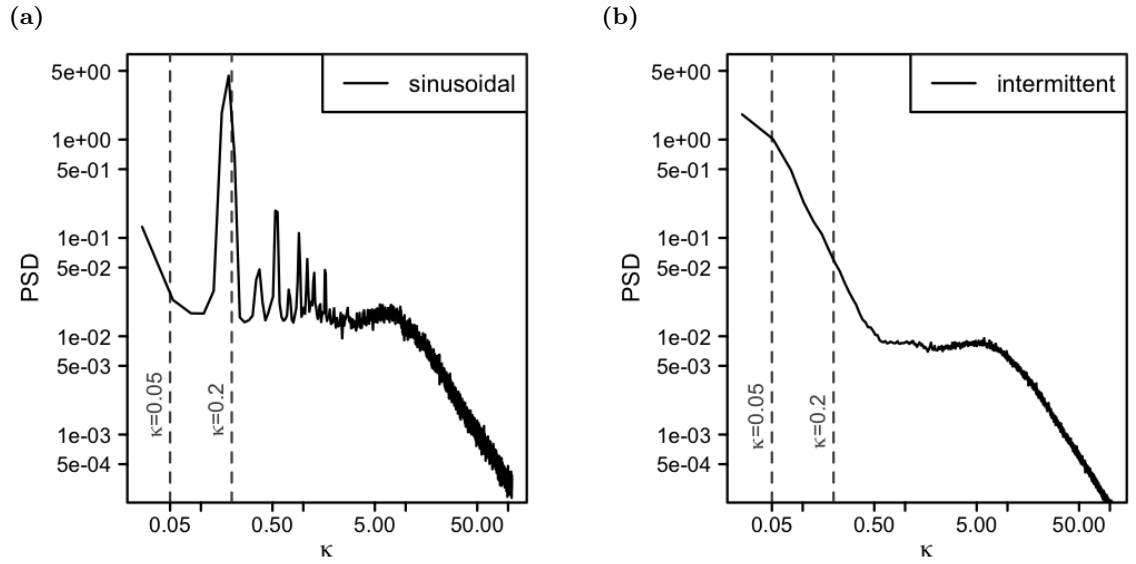

Figure 4. Power spectral density of the generated inflow angles at the airfoil position plotted against the reduced frequency κ for both turbulent grid protocols. The sinusoidal spectrum (a) features one dominant frequency $\kappa = 0.18$, while intermittent spectrum (b) covers a wider range of frequencies $\kappa \leq 0.5$. The reduced frequencies associated by Leishman [1] with unsteady ($\kappa = 0.05$) and highly unsteady flow ($\kappa = 0.2$) are marked with dashed lines.

4. Averaged Pressure Distributions and Polars

Pressure distributions of the airfoil with free transition were obtained for laminar inflow and for the two different types of inflow turbulence (sinusoidal, intermittent) at 71 angles of attack (AoA) within $\alpha = \pm 35°$. Temporal averaging of the data for each pressure tap was performed in order to obtain the average pressure distributions. The lift and drag forces L and D were used to calculate the corresponding lift and drag coefficients C_L and C_D according to standard definitions, given e.g. in [1]. The lift coefficients resulting from chord-wise pressure integration and the coefficients calculated from the higher resolved load cell data agree well in the linear region of the averaged lift polar, but the C_L from pressure integration is lower at maximum lift and in the stall region. Due to the absence of a wake rake in the performed experiments, no reliable drag coefficient could be computed from the pressure distributions. Thus, the lift and drag polars shown hereafter are based on the load cell data.

The time-averaged pressure distributions for the laminar case are shown in Figure 5 (a1) for three distinguished angles of attack α in the positive range. The maximum lift-to-drag ratio $L/D = 62$ occurs for $\alpha = 7.8°$. A kink in the pressure distribution can be seen at about x/c =0.45 originating from a laminar separation bubble. The occurrence of a separation bubble is not surprising at this rather low Reynolds number, since the DU airfoils are designed for $Re \approx 2 \ldots 4 \cdot 10^6$ [12]. As the AoA is increased to $\alpha = 9.8°$, the lift coefficient C_L is maximized with $C_{L,max} = 1.38$. The laminar separation bubble moves towards the leading edge and is found at $x/c \approx$0.35 for this AoA. The third curve for $\alpha = 15.8°$ is selected as a post-stall example, in which the flow above the upper airfoil surface can be considered fully separated for $x/c \geq 0.4$. A laminar separation bubble (LSB) cannot be clearly identified for this case, albeit it can be speculated to occur at $x/c \approx 0.04$. However, the spatial resolution of the pressure taps in this leading edge region seems to be too limited to confidently pinpoint its position.

Figure 5 (a2) shows the airfoil polars obtained from the time-averaged load cell data for each AoA. The characteristic angles of attack considered in Figure 5 (a1) can be found particularly in the lift polar, which shows a rather sharp transition to stall for the DU 00-W-212 airfoil beyond

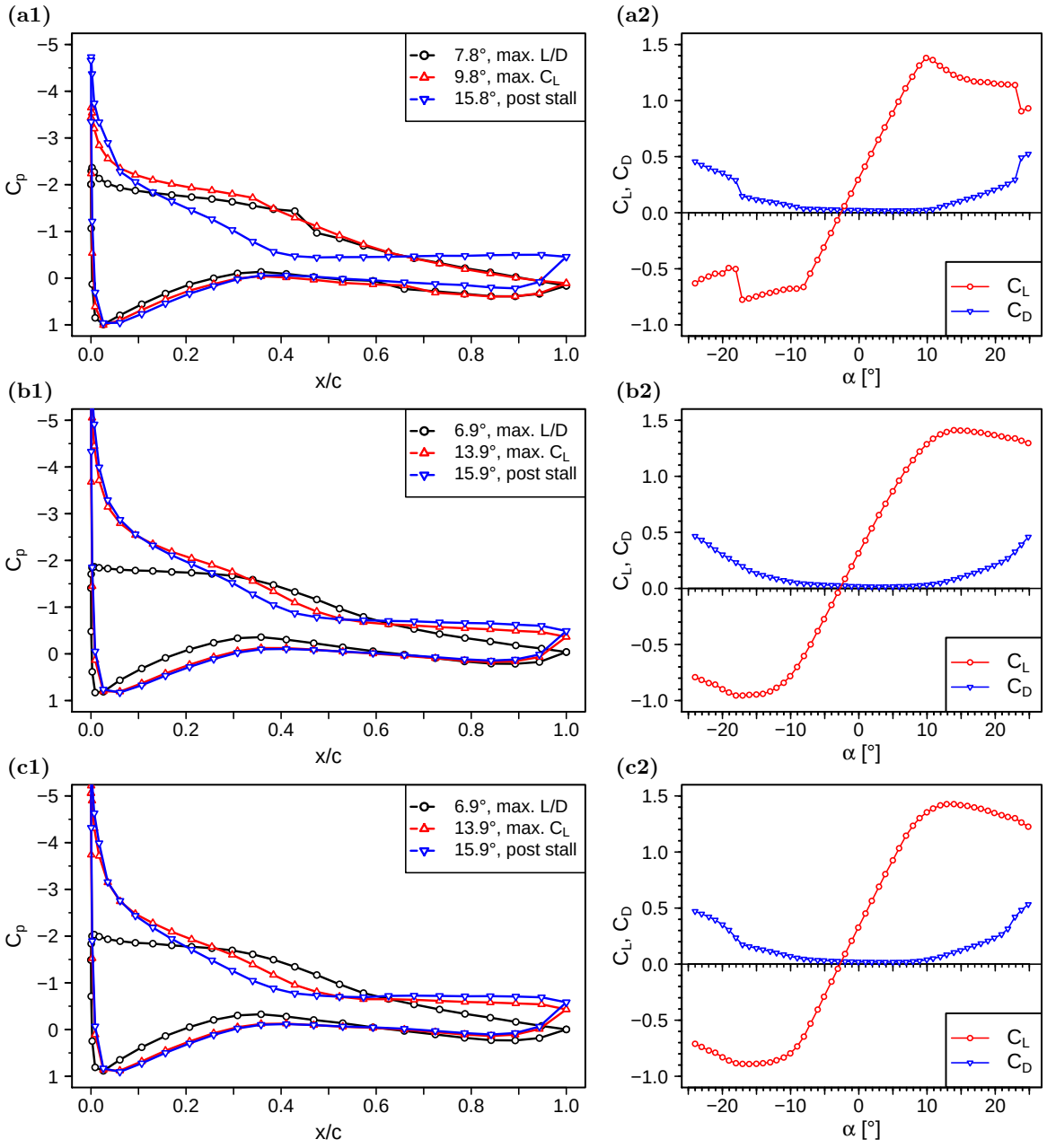

Figure 5. Chord-wise distributions of the pressure coefficient C_p at angles of attack α with maximum lift-to-drag ratio L/D, maximum C_L and post stall in laminar flow (a1), sinusoidal flow (b1) and intermittent flow (c1). The corresponding lift and drag polars measured with the load cells are shown in plots (a2), (b2) and (c2), respectively.

$\alpha = 10°$. A sudden drop in C_L is observed for $\alpha \approx 24°$ marking the onset of fully separated flow on the airfoil's suction side in deep stall.

Time-averaged pressure distributions and polars measured in turbulent inflow using the sinusoidal grid protocol are shown in Figures 5 (b1) and (b2), respectively. Similar cases, namely maximum L/D, maximum C_L and the AoA of the laminar post-stall case have been selected for comparison to the laminar baseline case. The pressure distribution for maximum L/D is found at a lower AoA, $\alpha = 6.9°$, with $L/D = 53$ also being reduced compared to the laminar case.

The maximum lift $C_{L,max}$ on the contrary is delayed to higher AoAs at $\alpha = 13.9°$ and the value of $C_{L,max} = 1.41$ is slightly increased. In comparison with the laminar inflow, the flow along the upper surface is slightly longer attached at $\alpha = 15.9°$ (Fig. 5 (b1)). The slope of the lift polar in Figure 5 (b2) is reduced while the stall region is smoothened and extended in comparison to the laminar case. No sudden onset of deep stall is found within the plotted range of $\alpha = \pm 25°$, but $\alpha \approx 29°$ is a reasonable estimate based on the full set of measured AoAs.

The pressure distributions of the intermittent cases for maximum L/D, maximum C_L and post-stall exhibit a slightly wider spread in their transition regions ($x/c \approx 0.2 \ldots 0.55$) compared to the sinusoidal inflow cases, but match quite well otherwise. For both turbulent inflow cases, neither of the evaluated AoAs features a laminar separation bubble in the pressure distribution, since the inflow is already turbulent and the considered data captures only the mean values of the pressure tap readings. Devinant et al. state that in cases of high background turbulence, transition may occur before laminar separation happens and consequently no laminar separation bubble is present [6]. It is therefore in accordance with the expectations, that no LSB is found in any of the time-averaged pressure distributions for the sinusoidal and the intermittent inflow turbulence. An analysis of the polars from the intermittent inflow protocol (Fig. (c2)) also leads to similar values of the angles of attack α for maximum lift-to-drag ratio L/D and maximum lift coefficient $C_{L,max}$ as found in the sinusoidal inflow case. The values for these characteristic quantities are summarized in Table 2. However, it is worth noting the large difference in maximum lift-to-drag ratio for sinusoidal (L/D =53) and intermittent (L/D =60) inflow even though the other values are found to be almost identical. Further investigations on this are necessary from more advanced data analysis and follow-up measurements. The slope of the linear region of the lift polar is not reduced as in the sinusoidal case, but the stall region has a similar extent although the drop in lift progresses slightly faster. Nevertheless, it is still significantly smoother than in the laminar baseline case.

Table 2. Characteristic quantities measured for the DU 00-W-212 airfoil with different inflows.

inflow	$\alpha_{(L/D),max}$	$(\frac{L}{D})_{max}$	$\alpha_{C_{L,max}}$	$C_{L,max}$	$\alpha_{C_L=0}$
laminar	7.8°	62	9.8°	1.38	-2.6°
sinusoidal	6.9°	53	13.9°	1.41	-2.8°
intermittent	6.9°	60	13.9°	1.43	-2.8°

Considering not only the mean values of the pressure tap measurements, but also the minimal and maximal readings through the course of the time series can serve as an indicator for variability of pressure distribution. A comparison of the pressure distributions for $\alpha \approx 8°$ is given in Figure 6. The error bars in this representation mark the minimal and maximal C_p of the respective pressure tap. For this AoA in the linear region of the lift polar, the extreme variations from the mean are relatively small in the laminar baseline case, while the variations are significantly increased in the turbulent cases. Moreover, large differences can be seen between the size of the error bars of the sinusoidal and intermittent cases. Although the intermittent inflow comprises a lower turbulence intensity $I_u = 3.7\%$ than the sinusoidal inflow with $I_u = 5.0\%$, the resulting C_p variations are more pronounced. The choice of the same AoA for the comparison of the pressure distributions, here $\alpha \approx 8°$, is one representative example for the described effect. Similar results are obtained for the comparison of pressure distributions at other AoAs as well as for the previously treated cases of $\alpha_{C_{L,max}}$ or $\alpha_{(L/D),max}$. The increased extreme values in the intermittent case can be attributed the occurrence of fewer but larger AoA variations compared to the sinusoidal case. Consequently, the comparison of the standard deviations for each case yields higher σ for the sinusoidal case due to the regular occurrence of the AoA variations. This can clearly be seen in the lift and drag polars shown in Figure 7. It is therefore not sufficient

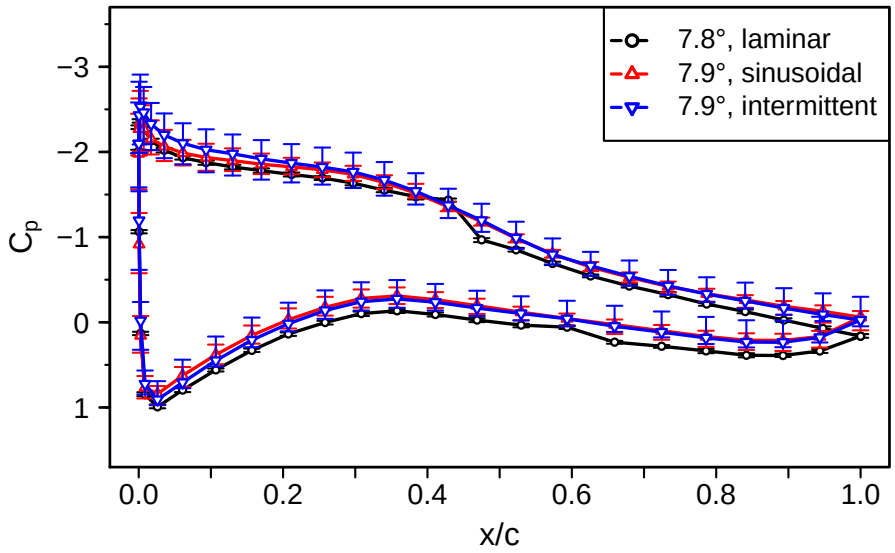

Figure 6. Comparison of the laminar inflow with both turbulent inflow cases. (a) Mean pressure distributions for all inflow patterns at $\alpha \approx 8°$. The error bars denote the minimum and maximum value of C_p from the pressure tap reading.

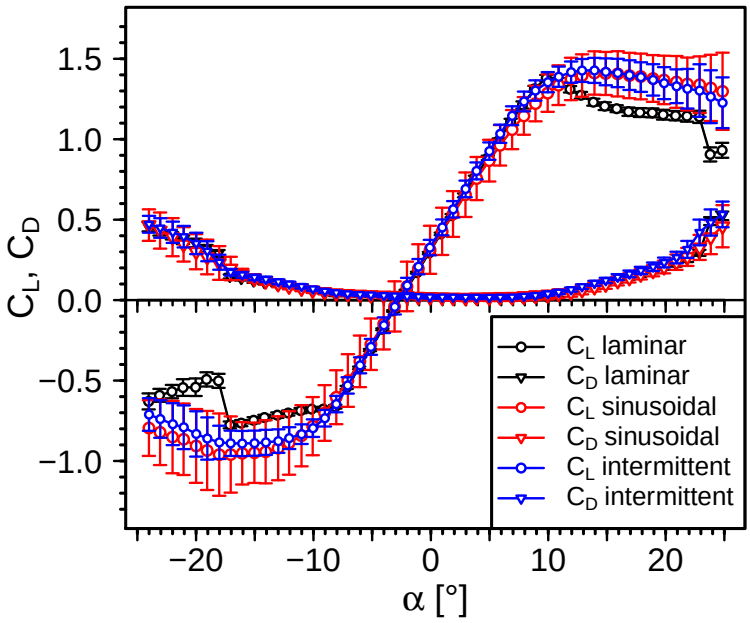

Figure 7. Comparison of the laminar inflow with both turbulent inflow cases. Lift and drag polars with standard deviations of C_L and C_D from load cell data.

to take only averages of the relevant quantities into account when the airfoil is exposed to turbulent flows of different characteristics but for a detailed analysis of the airfoil behavior the highly resolved data has to be considered.

5. Conclusion

Airfoil characteristics of a wind turbine dedicated DU 00-W-212 profile were measured in laminar and customized turbulent inflow conditions generated by using an active grid. The spectral characteristics of the sinusoidal inflow exhibits a pronounced reduced frequency peak, while the intermittent inflow has a wider reduced frequency distribution, which seems to fit wind turbine applications better. Comparisons of the averaged pressure distribution for distinguished AoAs with the laminar case show clear differences, e.g. the absence of a laminar separation bubble in the turbulent cases. The averaged lift polars indicate a slightly higher $C_{L,max}$ which occurs at higher AoAs and a significantly smoother transition to stall for the turbulent inflows. The stall region is also stretched and complete flow separation is delayed in both cases. A reduced slope of the linear region of the lift polar and an extended stall region are found for the sinusoidal inflow compared with the laminar and intermittent cases. This is in agreement with results from Devinant et al. [6], which attribute similar observations to a higher turbulence intensity.
The extrema of the pressure fluctuations were found to be higher in the intermittent case than in the sinusoidal case, although the latter has a higher turbulence intensity. A deeper analysis of the time-resolved data is therefore recommended to better grasp the impacts of the different inflows.

Acknowledgments

The presented work was performed within the project AVATAR and is funded from the European Unions Seventh Program for research, technological development and demonstration under grand agreement No FP7-ENERGY-2013-1/n 608396.
The authors gratefully appreciate the support of Jesper Madsen (LM WindPower) who provided the pressure tap layout. We also thank Tim Homeyer, Gerrit Kampers, Lars Kröger and Jannik Schottler for their assistance during the measurement campaign.

References

[1] Leishman J G 2006 *Principles of Helicopter Aerodynamics* 2nd ed Cambridge Aerospace Series (Cambridge University Press)
[2] Wolken-Möhlmann G, Knebel P, Barth S and Peinke J 2007 *Journal of Physics: Conference Series* **75** 012026 URL http://stacks.iop.org/1742-6596/75/i=1/a=012026
[3] Strangfeld C, Müller-Vahl H, Nayeri C N, Paschereit C O and Greenblatt D 2016 *Journal of Fluid Mechanics* **793** 79–108 URL http://dx.doi.org/10.1017/jfm.2016.126
[4] Wächter M, Heißelmann H, Hölling M, Morales A, Milan P, Mücke T, Peinke J, Reinke N and Rinn P 2012 *Journal of Turbulence* **13** N26 (*Preprint* http://www.tandfonline.com/doi/pdf/10.1080/14685248.2012.696118) URL http://www.tandfonline.com/doi/abs/10.1080/14685248.2012.696118
[5] Pereira R, Schepers G and Pavel M D 2013 *Wind Energy* **16** 207–219 ISSN 1099-1824 URL http://dx.doi.org/10.1002/we.541
[6] Devinant P, Laverne T and Hureau J 2002 *Journal of Wind Engineering and Industrial Aerodynamics* **90** 689–707 ISSN 0167-6105 URL http://www.sciencedirect.com/science/article/pii/S0167610502001629
[7] Sicot C, Aubrun S, Loyer S and Devinant P 2006 *Experiments in Fluids* **41** 641–648 ISSN 1432-1114 URL http://dx.doi.org/10.1007/s00348-006-0187-9
[8] Schneemann J, Knebel P, Milan P and Peinke J 2010 *Proceedings of EWEC 2010*
[9] Eisele O, Pechlivanoglou G, Nayeri C and Paschereit C 2013 *Proceedings of ASME Turbo Expo 2013: Turbine Technical Conference and Exposition*
[10] Knebel P, Kittel A and Peinke J 2011 *Experiments in Fluids* 1–11 ISSN 0723-4864 10.1007/s00348-011-1056-8 URL http://dx.doi.org/10.1007/s00348-011-1056-8
[11] Weitemeyer S, Reinke N, Peinke J and Hölling M 2013 *Fluid Dyn. Res.* **45** 061407 (16pp)
[12] Timmer W and van Rooij R 2003 *Journal of Solar Energy Engineering* **125**